Influence of strain rate and temperature on the mechanical behaviour of rubber-modified polypropylene and cross-linked polyethylene

Joakim Johnsen[a,*], Frode Grytten[b], Odd Sture Hopperstad[a], Arild Holm Clausen[a]

[a]*Structural Impact Laboratory (SIMLab), Department of Structural Engineering, NTNU, Norwegian University of Science and Technology, NO-7491 Trondheim, Norway*
[b]*SINTEF Materials and Chemistry, Department of Materials and Nanotechnology, PB 124 Blindern, NO-0314 Oslo, Norway*

Abstract

In the present work, we investigate the effects of strain rate ($\dot{e} = 0.01$ s^{-1}, 0.1 s^{-1}, and 1.0 s^{-1}) and low temperature ($T = -30$ °C, -15 °C, 0 °C, and 25 °C) on the mechanical behaviour in tension and compression of two materials: a rubber-modified polypropylene copolymer (PP) and a cross-linked low-density polyethylene (XLPE). Local stress-strain data for large deformations are obtained using digital image correlation (DIC) in the uniaxial tension tests and point tracking in the compression tests. Since both materials exhibit slight transverse anisotropy, two digital cameras are used to capture the strains on two perpendicular surfaces. Self-heating resulting from the elevated strain rates is monitored using an infrared (IR) camera. To enable the application of multiple digital cameras and an IR camera, a purpose-built transparent polycarbonate temperature chamber is used to create a cold environment for the tests. The mechanical behaviour of both materials, including the true stress-strain response and the volume change, is shown to be dependent on the temperature and strain rate. The dependence of the yield stress on the temperature and strain rate follows the Ree-Eyring flow theory for both materials, whereas Young's modulus increases with decreasing temperature for PP and XLPE and with increasing strain rate for XLPE. Furthermore, a scanning electron microscope (SEM) study was performed on both materials to get a qualitative understanding of the volumetric strains.

Keywords: Polyethylene, Polypropylene, Temperature, Strain rate, DIC, Tensile test, Compression test, Self-heating, Volume change

*Corresponding author
Email address:* `joakim.johnsen@ntnu.no` (Joakim Johnsen)

1. Introduction

In recent years, there has been increased interest in using polymeric materials in structural applications. The automotive industry, for example, is using polymeric materials in their pedestrian safety devices as sacrificial components that are designed to dissipate energy during impacts. An important point in this context is that material characterization and impact tests are performed close to room temperature, thus failing to account for changes in material behaviour as the temperature decreases. At low temperatures, polymeric materials tend to be both stiffer and more brittle, which could have severe consequences in a collision between a car and a pedestrian. Considering the cost of conducting prototype testing, it is clear that increased knowledge regarding the material behaviour at different temperatures is highly relevant.

The oil and gas industry is also interested in polymeric materials. As they continue to explore and search for oil and gas in harsher climates, new classification rules for materials are needed. There is an increasing need to understand how polymers behave at low temperatures due to this industry's expansion into the arctic region. There are various relevant structural applications for polymers in the oil industry, ranging from polymeric shock absorbers in load-bearing structures to gaskets used in pressurized components. In particular, for the two materials considered in this work, cross-linked low-density polyethylene (XLPE) is used as electrical insulation in high-voltage cables and as a liner material in flexible risers, while one application for rubber-modified polypropylene (PP) is thermal insulation of pipelines. As in the automotive industry, prototype testing is expensive; therefore, there is a demand for validated material models in finite element codes to reduce the number of experiments necessary to qualify a given material.

Reliable and good experimental data are a prerequisite for developing and improving phenomenological material models. At room temperature, the use of non-contact measuring devices to extract local stress-strain data from mechanical tests on polymeric materials has become widespread [1–3]. Digital image correlation (DIC) is an important tool because it enables local measurements of the strains (both longitudinal and transverse) in the neck of a tension test, which differs from an extensometer that provides average strains over a section. Therefore, by using DIC, local measurements of the volumetric strain are obtainable – a quantity that is useful for determining the plastic potential and for including damage modelling. However, when a temperature chamber is introduced, either to increase or decrease the temperature, the view of the specimen is obstructed. Most commercially available temperature chambers have only one window. This limits the number of possible digital cameras in the experimental set-up to one, thereby making the monitoring technique suitable only for isotropic materials. Consequently, many researchers use mechanical

2

measuring devices such as extensometers or machine displacement to obtain stress-strain data when using a temperature chamber. Such instrumentation protocols will only reveal the average strain over the gauge length. Nevertheless, using these measurement techniques, a number of studies [4–9] have investigated the effects of increased temperature and strain rate on the material behaviour. In all these studies, the typical polymer behaviour is observed, i.e., increasing the strain rate increases the yield stress, whereas increasing the temperature decreases the yield stress. However, only the study by Arruda et al. [4] was conducted using an infrared (IR) sensor to measure self-heating at elevated strain rates, while none of the studies [4–9] report the volumetric strain. Similar studies considering the material behaviour at low temperatures [10–14] report the same trend – decreasing the temperature and increasing the strain rate increases the yield stress. As for the studies at elevated temperatures, the strain calculation relies on mechanical measurement techniques. Neither self-heating nor change in volume is reported in any of these studies.

Previous studies have been conducted on materials comparable to the two materials of interest in our study. For instance, Ponçot et al. [15] studied the volumetric strain at different strain rates in a polypropylene/ethylene-propylene rubber using a VideoTraction system. Their results are similar to the results obtained for the rubber-modified polypropylene material investigated in our study. Using a linear variable differential transformer to measure the cross-head displacement, Jordan et al. [16] conducted compression tests on low density polyethylene (LDPE) at four different temperatures and eight strain rates. Considering the effect on the yield stress, they found that an order of magnitude change in strain rate is approximately equal to a 10 degree change in temperature. An extensive study on a cross-linked polyethylene (PEX) was conducted by Brown et al. [17] utilizing a displacement extensometer. In their study, compression tests were conducted at temperatures ranging from -75 °C to 100 °C, and strain rates from 10^{-4} s^{-1} to 2650 s^{-1}. Addiego et al. [18] characterized the volumetric strain in HDPE through uniaxial tension and loading/unloading experiments at room temperature and strain rates from 10^{-4} s^{-1} to $5 \cdot 10^{-3}$ s^{-1}, using the same VideoTraction system as Ponçot et al. [15].

Conventional temperature chambers also exclude the possibility of using an IR camera because a free line-of-sight between the specimen and the IR camera is required. Since polymers become softer at elevated temperatures, monitoring self-heating during a test is essential to successfully separate the effects of strengthening due to rate sensitivity and softening due to increasing temperature. An experimental set-up that circumvents the limitations imposed by using a conventional temperature chamber was presented by Johnsen et al. [19]. Here, a transparent polycarbonate (PC) temperature chamber was used, facilitating the

3

use of multiple digital cameras to monitor the specimen during deformation. In addition, a slit was added in one of the chamber walls to obtain a free line-of-sight between an IR camera and the test specimen.

This polycarbonate temperature chamber was used in the present work, where the Cauchy stress, the logarithmic strain tensor and self-heating were obtained from uniaxial tension tests performed on two different materials: a rubber-modified polypropylene and a cross-linked low-density polyethylene. The tests were performed at four temperatures ($-30\,°C$, $-15\,°C$, $0\,°C$ and $25\,°C$) and three nominal strain rates ($0.01\,\text{s}^{-1}$, $0.1\,\text{s}^{-1}$ and $1.0\,\text{s}^{-1}$), and all experiments were monitored by two digital cameras and a thermal camera. The two digital cameras were used to obtain local measurements of the longitudinal and transverse strains on two perpendicular surfaces of the axisymmetric tensile specimen, allowing us to calculate the Cauchy stress and the volumetric strain during the entire deformation process. The strains, along with the thermal history, were extracted at the point of initial necking, thus providing us with the temperature change as a function of logarithmic longitudinal strain. These are all vital quantities in material model calibration. The volumetric strain may be used in damage modelling, the thermal history may be linked to strain softening, and the variation of temperature and strain rate may provide the temperature and rate sensitivity, e.g. through the Ree-Eyring model [20]. To obtain a qualitative understanding of the volume change, some scanning electron microscopy (SEM) micrographs are also presented herein.

Furthermore, uniaxial compression tests were performed at the same temperatures and strain rates to investigate the pressure sensitivity of the two materials. The combined information from the uniaxial tension and compression tests allows us to study any pressure sensitivity of the materials, a phenomenon that is caused by the reduced molecular mobility under compression compared to that under tension [21]. Another source for this pressure sensitivity may be the existence, or nucleation, of voids in the material [22]. Stretching the material will cause the voids to grow, thus reducing the density of the bulk material, whereas compressing the material will have the opposite effect. Consequently, this leads to different material response in the two deformation modes.

2. Materials and methods

2.1. Materials

Two materials produced by Borealis were investigated: a rubber-modified polypropylene (PP) with the product name EA165E [23] and a cross-linked low-density polyethylene (XLPE) with the product name LS4201S [24]. The polypropylene material was received directly from Borealis as an extruded pipe with

4

dimensions of 1000 mm × 250 mm × 22 mm (length × diameter × thickness), whereas the XLPE material was received from Nexans Norway as high-voltage cable segments in which the copper conductor had been removed. The dimensions of the cable insulation were 128 mm × 73 mm × 22.5 mm (length × diameter × thickness).

The physical properties of both materials are presented in Table 1. The densities were found from the datasheets supplied with the materials, whereas the specific heat capacity C_p and the thermal conductivity k were determined using the laser flash method [25]. Five circular samples with dimensions of 12.7 mm × 0.5 mm (diameter × thickness) of each material were heated to three temperatures: 25 °C, 35 °C, and 50 °C. Subsequently, the specific heat capacity and thermal conductivity were measured at each temperature level. The specific heat capacity increased almost linearly with temperature, whereas the thermal conductivity exhibited little variation. The values presented in Table 1 are the values obtained at room temperature. Heat convection to air, h_c, was determined by heating a small cylindrical sample with dimensions of 20 mm × 5 mm (diameter × height) in boiling water. The temperature decay was monitored using an infrared thermometer, and the heat convection to air was then calculated from the temperature-time history.

2.2. Test specimens

Axisymmetric specimens were used for both the tensile tests and the compression tests on the PP and XLPE materials. However, since the XLPE is softer than the PP, it was not possible to machine threads into the grips of the XLPE tensile specimens. The test specimens are illustrated in Figure 1.

All specimens were machined in a turning lathe from sections cut from the longitudinal direction of the extruded PP pipe and the extruded XLPE cable insulation. The radial direction was marked on the test specimens such that it could be distinguished from the hoop direction when the specimen was mounted in the test rig, see Figure 2.

2.3. Experimental set-up and program

All experiments were performed in an Instron 5944 testing machine with a 2 kN load cell. A key component in the experimental set-up, see Figure 3, was a transparent polycarbonate (PC) chamber, which allowed for non-contact optical devices to monitor local deformations during testing. Two Prosilica GC2450 digital cameras equipped with Sigma 105 mm and Nikon 105 mm lenses were used in this study. Both cameras were mounted between 25 cm and 35 cm from the tensile specimen, equating to a resolution of approximately 60 pixels/mm. For the compression tests, the cameras were mounted approximately 10 cm

away from the specimens, yielding a resolution of approximately 190 pixels/mm. Due to slight transverse anisotropy, see Figure 4, the two digital cameras, mounted perpendicular to each other, were used to monitor the surfaces normal to the radial and hoop directions of the specimens, see Figures 2 and 3. Consequently, it was possible to obtain the longitudinal strain and the transverse strain in the radial and hoop directions of the extruded PP pipe and the XLPE cable insulation. In addition, a FLIR SC 7500 thermal camera, measuring temperatures down to $-20\,°C$, was used to monitor self-heating in the test specimens during all uniaxial tension tests. A slit was added in the front window of the chamber (as indicated in Figure 3) to obtain a free line-of-sight between the test specimen and the thermal camera. A thermocouple temperature sensor mounted close to the test specimen was used to control the flow of liquid nitrogen into the chamber, and fans continuously blew air over the chamber walls to prevent condensation. The test specimens were thermally conditioned at the desired temperature for a minimum of 30 minutes prior to testing. A detailed description of the temperature chamber along with the experimental set-up is given by Johnsen et al. [19].

In the uniaxial tension tests at room temperature, a black and white spray-paint speckle was applied on the specimen surface. However, at the lower temperatures, the spray-paint speckle cracked and was therefore replaced with white grease and black powder. The black and white speckle is needed to perform digital image correlation (DIC) analyses of the images after the experiment. All uniaxial tension tests were post-processed using the in-house DIC code µDIC [26]. In the compression tests, point tracking (subsets) was used to follow two points on the specimen surface to calculate the longitudinal strain, whereas edge tracing was used to determine the transverse strains. Another in-house DIC code, eCorr [27], was used to track the points on the surface of the compression specimen, and MATLAB was used to trace the edges. To reduce friction between the test machine and the compression specimen, PTFE tape and oil were used at the two highest temperatures ($25\,°C$ and $0\,°C$). At the two lowest temperatures ($-15\,°C$ and $-30\,°C$), however, the oil was replaced with grease. Note that the specimen moved horizontally during some compression tests at the lowest temperatures and highest strain rates. In these tests, the lubrication was completely removed, and then the test was repeated. Photos of representative tensile and compression specimens with black and white speckle and surface points are shown in Figure 5.

Uniaxial tension and compression tests were performed at four different temperatures T of $25\,°C$ (room temperature), $0\,°C$, $-15\,°C$, and $-30\,°C$, and three different nominal strain rates $\dot{e}$ of $0.01\,\mathrm{s}^{-1}$, $0.1\,\mathrm{s}^{-1}$, and $1.0\,\mathrm{s}^{-1}$, corresponding to cross-head velocities v of $0.04\,\mathrm{mm/s}$, $0.4\,\mathrm{mm/s}$ and $4.0\,\mathrm{mm/s}$, respectively. The

initial nominal strain rate was calculated as

$$\dot{e} = \frac{v}{L} \tag{1}$$

where v is the test machine's cross-head velocity and L is the length of the parallel section (gauge) of the test specimen. Figures 6a and 6b shows the local logarithmic strain rate ($\dot{\varepsilon}_L$) in the section experiencing the first onset of necking as a function of longitudinal strain for both the XLPE and the PP material, respectively. Contrary to expectations the local logarithmic strain rate does not exceed the initial nominal strain rate. A possible explanation is that the effective length of the parallel section of the tensile specimen, L, is slightly higher than 4 mm, causing the strain rate to decrease. For each test configuration, a minimum of two replicate tests were performed. A third test was conducted if a significant deviation was observed in the force-displacement curves between the two replicate tests. Although there was some variation in the fracture strain between the replicate tensile tests, there were only small differences in the stress-strain curve. In the replicate compression tests, there was some variation in the stress-strain curve after yielding but close to no variation in the magnitude of the yield stress. The clamping length of the specimens in the uniaxial tension tests was approximately 20 mm.

2.4. Calculation of Cauchy stress and logarithmic strain

Two digital cameras were used to monitor the deformation in the radial and hoop directions of the test specimen, with respect to the extruded PP pipe and XLPE cable insulation, see Figure 2. In the tension experiments, the section of initial necking was found on each surface, and the strain components were extracted at this section throughout the test. This ensured that the same point was tracked throughout the experiment, and that the strains from the two surfaces were obtained from the same point on the specimen. In the compression tests, the longitudinal strain were obtained from the distance between the highlighted points in Figure 5b, while the transverse strain on each surface was found by identifying the section of maximum diameter throughout the experiment. For both loading modes, the transverse stretches measured by each of the digital cameras were assumed to represent the stretches along the minor and major axes of an elliptical cross-section, enabling the calculation of the current cross-sectional area of the specimen as

$$A = \pi r_0^2 \cdot \frac{r_R}{r_0} \cdot \frac{r_H}{r_0} = \pi r_0^2 \lambda_R \lambda_H \tag{2}$$

where r_0 is the initial radius of the specimen; r_R and r_H are the radii in the radial and hoop directions, respectively; λ_R is the transverse stretch in the radial direction; and λ_H is the transverse stretch in the

perpendicular hoop direction, see Figure 2. Using the transverse stretches from each camera, the volumetric strain is determined as

$$\varepsilon_V = \ln\left(\lambda_L \lambda_R \lambda_H\right) \tag{3}$$

where λ_L is the longitudinal stretch. The logarithmic strain components are calculated by taking the natural logarithm of the corresponding stretch component, i.e., $\varepsilon_i = \ln\left(\lambda_i\right)$. Note that we only obtain the strains on the surface of the specimen from the experiments. Thus, using Equation (3) to calculate the volumetric strain, we assume a homogeneous strain field over the cross-section. This assumption is only valid until the point of necking, where the strain field (and the stress field) becomes heterogeneous. The implications of this assumption are further discussed in Section 4. Using the expression for the area in Equation (2), the average Cauchy stress can be calculated as

$$\sigma = \frac{F}{A} \tag{4}$$

where F is the force measured by the testing machine.

Note that the yield stress (σ_0) throughout this study is taken to be equal to the flow stress at a longitudinal logarithmic strain of 0.15 (15%). A logarithmic strain of 0.15 was chosen because the material exhibits plastic flow at that point, while it is still close to the yield point. This definition of the yield stress applies for both tension and compression.

2.5. Calculation of self-heating

A MATLAB routine was established to obtain the temperature change on the surface of the tensile specimen at approximately the same position as the strains were extracted. Figure 7 shows a snapshot of the temperature field, alongside the strain field for the PP material tested at room temperature and the highest strain rate. As indicated in the figure, the temperature gradient, ∇T, is calculated along a row of pixels (denoted row A in Figure 7) containing the top and bottom of the specimen, with air in-between. Since the temperature of the surrounding air is constant, an abrupt change in the temperature gradient will occur when transitioning from air to the specimen in the considered row of pixels. This allowed us to obtain the position of the top and bottom of the tensile specimen numerically, which again gave us the vertical coordinate, y_c, of the centre of the specimen during the experiment. The temperature is then extracted at the point (x_c, y_c) highlighted with a square in Figure 7, where x_c is the horizontal coordinate of the centre provided as user input. Note that the symbol T is used for all temperatures measured in degrees Celsius (°C) throughout the paper, while θ is applied for temperatures measured in Kelvin (K).

8

3. Results

3.1. Cross-linked low-density polyethylene (XLPE)

3.1.1. Uniaxial tension

Figure 8 presents the Cauchy stress plotted against the longitudinal logarithmic strain until fracture for uniaxial tension tests performed at four different temperatures (25 °C, 0 °C, −15 °C, and −30 °C) and three different initial nominal strain rates (0.01 s^{-1}, 0.1 s^{-1}, and 1.0 s^{-1}). Except for the lowest temperature, the stress-strain curves exhibit the same features: (1) a close to linear elastic behaviour up to the yield stress, (2) quasi-linear strain hardening, and (3) network hardening caused by the alignment of the polymer chains. At the lowest temperature, the network hardening is less prominent, and it appears to have completely vanished at the highest strain rate, as shown in Figure 8d.

By comparing Figures 8a through 8d, it is clearly observed that there is a strong increase in both the yield stress and the elastic stiffness as the temperature decreases. The yield stress at the lowest strain rate increases from approximately 10 MPa at room temperature (T = 25 °C) to approximately 30 MPa at the lowest temperature (T = −30 °C). As will be further discussed in Section 4, the dependence of the yield stress on strain rate and temperature obeys the Ree-Eyring flow theory [20]. The same trend is observed for the elastic stiffness: decreasing the temperature increases Young's modulus from approximately 200 MPa at room temperature to approximately 800 MPa at −30 °C. As for the yield stress, a dependence on strain rate is also evident for Young's modulus.

The locking stretch is taken as the stretch where the slope of the strain hardening curve increases significantly, see Figure 8a. As shown in Figures 8a to 8c, the locking stretch increases with strain rate. This behaviour is believed to be caused by self-heating in the material at higher strain rates, which increases the chain mobility and extends the cold drawing domain. By inspecting the locking stretch in the experiments conducted at the lowest strain rate, which will later be shown to yield isothermal conditions, i.e., no self-heating, it is also observed that the locking stretch remains relatively constant down to a temperature of −15 °C. At the lowest temperature of −30 °C, no apparent locking stretch was detectable, see Figure 8d.

By applying Equation (3), the volumetric strains of XLPE at the investigated temperatures and strain rates are shown in Figure 9. Because of how the strain components are obtained from the experiments, an unphysical negative volumetric strain is observed at the beginning of each test. This discrepancy will be further discussed in Section 4. Nevertheless, Figure 9a shows that the polyethylene material is nearly incompressible for all the investigated strain rates at room temperature. This observation is further supported

9

by the scanning electron microscopy (SEM) micrograph presented in Figure 10, where it is observed that the material contains few particles and, except for a few small cracks, is free of voids. At the three lowest temperatures, however, the volumetric strain increases to between 0.08 and 0.1. Note that the increasing negative volumetric strain at the beginning is due to the formation of a more pronounced neck, leading to a more heterogeneous strain field through the necked cross-section.

Figure 11 shows the self-heating in the XLPE material during deformation. At the lowest strain rate ($\dot{e} = 0.01$ s^{-1}), we have isothermal conditions for all investigated temperatures. The reason for why there are no data points from the test performed at the lowest temperature ($T = -30$ °C) is that the infrared camera only records temperatures that are higher than -20 °C. At the intermediate strain rate ($\dot{e} = 0.1$ s^{-1}), we observe a temperature increase due to self-heating of approximately 10 °C, whereas at the highest strain rate a temperature increase of approximately 20 °C to 30 °C is observed. The self-heating increases with reduced initial temperature.

3.1.2. Uniaxial compression

Uniaxial compression tests were performed at the same temperatures (25 °C, 0 °C, −15 °C, and −30 °C) and initial nominal strain rates (0.01 s^{-1}, 0.1 s^{-1}, and 1.0 s^{-1}) as the tension tests. A comparison of the Cauchy stress vs. logarithmic strain curves for uniaxial compression and tension at $T = 25$ °C is presented in Figure 12. As shown, the pressure sensitivity, defined as the ratio between the compressive and tensile yield stress, $\alpha_{\mathrm{p}} = \sigma_{\mathrm{C}}/\sigma_{\mathrm{T}}$, is negligible for the polyethylene material. Conversely, the hardening is slightly higher in compression than in tension. However, note that barrelling occurred quite early in all the compression tests. Thus, the only purpose of the compression tests was to investigate the pressure sensitivity of the material in terms of the yield stress. A comparison of the compressive and tensile yield stress as functions of temperature and strain rate is shown in Figure 13. Similar to the observations from the uniaxial tension experiments, there is an increase in the compressive yield stress when decreasing the temperature and when increasing the strain rate.

The pressure sensitivity parameter $\alpha_{\mathrm{p}} = \sigma_{\mathrm{C}}/\sigma_{\mathrm{T}}$ is presented in Table 2 for all combinations of temperature and strain rate. Because α_{p} is consistently close to unity, the pressure sensitivity of the XLPE material is low.

3.2. Rubber-modified polypropylene (PP)

3.2.1. Uniaxial tension

The Cauchy stress vs. logarithmic strain curves from the tension tests of the polypropylene material are presented in Figure 14. Similar to the experiments conducted on the XLPE material, four temperatures (25 °C, 0 °C, −15 °C, and −30 °C) and three initial nominal strain rates (0.01 s^{-1}, 0.1 s^{-1}, and 1.0 s^{-1}) were investigated. The shape of the stress-strain curve for the two lowest strain rates is relatively the same for all temperatures: first a close to linear elastic behaviour up to a yield point, followed by strain hardening and ultimately asymptotic network hardening. At the highest strain rate and the three lowest temperatures, however, the material fractured before the locking stretch was reached.

In terms of the yield stress, the equivalence principle [28] holds, i.e., either reducing the temperature or increasing the strain rate increases the yield stress. At room temperature and for the lowest strain rate, the yield stress is approximately 20 MPa, while it has increased to approximately 24 MPa for the highest strain rate. At the lowest temperature, the quasi-static yield stress is approximately 35 MPa and increases to approximately 45 MPa for the highest strain rate, indicating that the rate-sensitivity is slightly higher at lower temperatures. The elastic modulus, however, exhibits little dependence on the strain rate, but it changes drastically with temperature. At room temperature, Young's modulus is approximately 850 MPa, whereas it has increased to approximately 2600 MPa at the lowest temperature.

As shown in Figure 15, the volumetric strains for the polypropylene material are considerably larger than those for XLPE and attain values between 0.5 and 0.9. At the two lowest strain rates, the shape of the curve is the same for all temperatures: first a significant evolution of volumetric strain up to a peak value followed by decreasing volumetric strain. Ponçot et al. [15] reported a similar observation on a comparable material (polypropylene/ethylene-propylene rubber). This result is due to the formation of voids in the material, believed to be initiated by cavitation in the rubbery phase of the rubber-modified polypropylene. Since there are no particles in these voids, they are not restrained against collapsing, which explains the decreasing volumetric strains after the peak value is reached. To investigate this assumption, two specimens were loaded in uniaxial tension at room temperature and a strain rate of 0.01 s^{-1} and thereafter unloaded; one specimen was unloaded before the maximum volumetric strain was reached, and the other one was unloaded after the maximum volumetric strain. SEM micrographs of the two samples are presented in Figures 16a and 16b. It appears from Figure 16 that the voids become elongated and start to close after the maximum volumetric strain is reached. At the highest strain rate, however, it seems that the voids do

11

not collapse at the three lowest temperatures, leading to a monotonically increasing volumetric strain up to fracture, as shown in Figures 15b to 15d.

The self-heating during the tensile experiments is presented in Figure 17. At the lowest strain rate, isothermal conditions prevail at all temperatures. As previously mentioned, there are no data points for the temperature change in the material at the lowest temperature ($T = -30$ °C) and the lowest strain rate due to the infrared camera being limited to temperatures above -20 °C. At the intermediate strain rate ($\dot{e} = 0.10$ s^{-1}), a temperature increase between 15 °C and 30 °C is observed before the temperature begins to decrease in the material. This decrease in temperature is due to the formation of a stable neck leading to cold drawing. This provides the material with enough time to conduct heat within the specimen and to convect heat to the surroundings. Although we have cold drawing at the highest strain rate ($\dot{e} = 1.0$ s^{-1}) at room temperature, the duration of the test is too short to allow for heat conduction or convection. This leads to the continuously increasing temperature for the highest strain rate at all temperatures in Figure 17. In contrast to XLPE, the temperature increase is approximately the same for all temperatures, i.e., between 40 and 50 °C, when adiabatic heating conditions are met.

Another observation is that the self-heating introduces a softening in the material, as indicated by the crossing of the stress-strain curves observed, for instance in Figure 14a. The self-heating increases the locking stretch for higher strain rates. Unlike XLPE, however, the opposite effect is observed when decreasing the temperature at the lowest strain rate, i.e., there is a reduction of the locking stretch for PP with decreasing temperature.

3.2.2. Uniaxial compression

Similar to the XLPE material, compression tests were performed for the PP material at four temperatures (25 °C, 0 °C, -15 °C, and -30 °C) and three initial nominal strain rates (0.01 s^{-1}, 0.1 s^{-1} and 1.0 s^{-1}). Figure 18 compares the stress-strain curves in uniaxial compression and tension at room temperature. It is clearly observed from the difference in compressive and tensile yield stress that the pressure sensitivity of the PP material is strong. Similar to the compression tests performed on the XLPE material, the onset of barrelling occurred for quite small deformations. Consequently, the compression tests were only conducted to determine the yield stress. As in tension, it is observed that higher strain rates and lower temperatures increase the yield stress in compression. The yield stresses in compression and tension are plotted as functions of temperature in Figure 19 for all the investigated strain rates.

The pressure sensitivity parameter $\alpha_{\mathrm{p}} = \sigma_{\mathrm{C}}/\sigma_{\mathrm{T}}$ is presented in Table 3 for all combinations of tem-

perature and strain rate. In contrast to the XLPE material, the pressure sensitivity is very high for the rubber-modified polypropylene. It is also observed that the pressure sensitivity increases at low temperatures.

4. Discussion

4.1. Temperature measurements

An infrared camera was employed to measure self-heating during the tests, see Section 2.3. In all experiments an emissivity of 0.95 was used. As validation, a uniaxial tension test at room temperature ($T = 25\ °C$) and at the highest strain rate ($\dot{e} = 1.0\ s^{-1}$) was performed on the XLPE material where the surface facing the thermal camera was coated with a black paint with an emissivity close to 1.0. The temperature as a function of longitudinal strain was then compared with a similar experiment where only a black and white speckle was applied. As evident from Figure 11a the difference between the measured self-heating for the two tests at the highest strain rate is minimal. Another possible issue is that the grease applied to the samples tested at low temperatures may affect thermal measurements. To validate the calculated self-heating from tests performed on materials coated with white grease, two tests at the highest strain rate were performed on the PP material at room temperature. In one of the tests a black and white spray paint speckle was applied, while in the other a white grease was used. The difference in self-heating, as shown in Figure 17a, was found to be negligible.

4.2. Young's modulus

Young's modulus as a function of temperature and strain rate is presented in Figures 20 and 21 for XLPE and PP, respectively. Young's modulus of the XLPE material was found through a linear fit of the stress-strain curve up to a longitudinal strain of $\varepsilon_L = 0.025$. For the PP material, Young's modulus was obtained by a linear fit of the stress-strain curve for $\sigma \in [0, 0.5\sigma_0]$, where σ_0 is the quasi-static yield stress at the investigated temperature. Due to noise in the strain values obtained from DIC, it was necessary to average the strain values over a larger area of the parallel section of the tensile specimen for the PP material. This can be done since the strain field remains homogeneous for the part of the stress-strain curve used to obtain Young's modulus.

For both materials, the elastic stiffness was found to be strongly dependent on the temperature. In XLPE, the elastic stiffness increases by a factor of 4: from approximately 200 MPa at room temperature to 800 MPa at $-30\ °C$. For the PP material, Young's modulus increases more than threefold: from approximately 850

13

MPa at room temperature to 2600 MPa at −30 °C. The temperature dependence within the experimental range is described using the same expression as Arruda et al. [4], i.e.

$$E(\theta) = E_0 \cdot \exp\left[-a\left(\theta - \theta_0\right)\right] \tag{5}$$

where θ_0 is the reference temperature, E_0 is Young's modulus at the reference temperature, a is a material parameter, and θ is the absolute temperature. The least squares fits of Equation (5) to the experimentally obtained Young's modulus for the materials at the lowest strain rate are shown in Figures 20 and 21, with $E_0 = 141$ MPa and $a = 0.03$ K^{-1} for the XLPE material, $E_0 = 842$ MPa and $a = 0.021$ K^{-1} for the PP material, and $\theta_0 = 298.15$ K (room temperature) for both materials.

Young's modulus was also found to be influenced by strain rate for the XLPE material, as shown in Figure 20. The trend of the elastic stiffness with respect to the rate sensitivity is not as clear for the PP material, as indicated in Figure 21. Since both Young's modulus and the yield stress is higher in PP compared to XLPE, this observation could be an artefact of the acceleration of the test machine, meaning that some time is needed before the cross-head reaches the desired velocity, or due to some slack in, e.g., the load cell or the grip. These factors, combined with a limited number of data points before yield for the two highest strain rates, could explain the discrepancies observed in Figure 21. Nevertheless, given that the most influential factor for both materials was the temperature, the strain rate dependence has been omitted in Equation (5).

4.3. Yield stress and pressure sensitivity

The Ree-Eyring flow theory [20] is frequently applied to model the influence of temperature and strain rate on the yield stress. Following the work of Senden et al. [29], a double Ree-Eyring model that includes both the main α relaxation and the secondary β relaxation is employed for evaluation and discussion of the experimental findings herein. Assuming that the contributions from each relaxation process are additive, the equivalent stress is given as

$$\bar{\sigma}(\dot{p}, \theta) = \sum_{x=\alpha,\beta} \frac{k_B \theta}{V_x} \operatorname{arcsinh}\left(\frac{\dot{p}}{\dot{p}_{0,x}} \exp\left[\frac{\Delta H_x}{R\theta}\right]\right) \tag{6}$$

Here, k_B is Boltzmann's constant, R is the gas constant, $\dot{p}$ is the equivalent plastic strain rate, θ is the absolute temperature, V_x ($x = \{\alpha, \beta\}$) is the activation volume, $\dot{p}_{0,x}$ is a local reference plastic strain rate, and ΔH_x is the activation enthalpy. For the purpose of obtaining the relation between the yield stress, temperature and strain rate, the equivalent stress $\bar{\sigma}$ is taken to be equal to the yield stress σ_0, and $\dot{p}$ is assumed to be equal to the initial nominal strain rate $\dot{e}$. The material parameters obtained from a least squares fit of Equation (6) to

14

the experimental data are presented in Table 4. All material parameters from the least squares fit appear to be reasonable from a physical perspective: the activation volume is between 1 nm^3 and 5 nm^3, the activation enthalpy ranges from 100 kJ/mol to 300 kJ/mol, and the local reference plastic strain rate attains values between 10^{17} s^{-1} and 10^{38} s^{-1}. The orders of magnitude are comparable to those of parameters reported for other materials in the literature, e.g. [10, 29]. Addressing the yield stress in tension, it appears from Figures 22 and 23 that the model captures the temperature and strain rate dependence of both materials excellently. Thus, the double Ree-Eyring model appears to be a promising choice for a thermomechanical description of the flow process of the materials at hand.

The pressure sensitivity parameter $\alpha_p = \sigma_C/\sigma_T$ is given in Tables 2 and 3 for the two materials. For the polyethylene material, which exhibits rather small volumetric strains, the pressure sensitivity is low, and α_p is close to unity. In contrast, the pressure sensitivity of the polypropylene material, which exhibits large volumetric strains, is high, and α_p ranges from 1.22 to 1.71. This result suggests that the lower yield stress in tension could be caused by the nucleation and growth of voids in the PP material. This assumption is supported by Lazzeri and Bucknall [21]. However, note that neither cavitation nor initial voids are prerequisites for a pressure-dependent material. In solid polymers, pressure dependence may arise from the fact that compression reduces the molecular mobility compared to tension, which increases the yield stress [21].

4.4. Volumetric strain

The negative volumetric strain observed for the polyethylene material, as shown in Figure 9, is due to the way in which it is calculated, i.e., we assume that the strain components calculated on the surface of the specimen are representative for the entire cross-section. This assumption is true only for homogeneous deformation, which occurs prior to necking. When the material necks, however, the strain components vary over the cross-section. The longitudinal strain component is largest in the centre of the specimen and smallest at the surface. This variation is not accounted for in our calculations and thus leads to an increasingly negative volumetric strain for test configurations where the external curvature of the neck, and thus the heterogeneity of the longitudinal strain, increases. This counter-intuitive and fictitious result can be remedied by accounting for the variation in the longitudinal strain over the cross-section, for instance, by assuming a parabolic distribution of the strain. Using this assumption, Andersen [26] obtained a formula for the corrected volumetric strain, viz.

$$\varepsilon_{V,corr} = \ln \left[\lambda_L \lambda_R \lambda_H \left(\frac{\kappa R}{4} + 1 \right) \right] \tag{7}$$

15

where κ is the external curvature of the neck and R is the radius in the neck. This correction removes the observed unphysical negative volumetric strain, as shown in Johnsen et al. [19]. Both geometrical measures κ and R can in principle be extracted from the digital pictures. In our case, however, the use of grease and black powder on the surface of the tensile specimens prohibited determination of the external curvature; therefore, the volumetric strain was calculated according to Equation (3).

Both materials have a fairly high linear thermal expansion coefficient α_T, which ranges between $146 \cdot 10^{-6}$ K^{-1} and $180 \cdot 10^{-6}$ K^{-1} for polypropylene and from $180 \cdot 10^{-6}$ K^{-1} to $400 \cdot 10^{-6}$ K^{-1} for low-density polyethylene [30]. Thus, the substantial self-heating may provide a significant contribution to the observed dilatation. The thermal volumetric strain is defined as

$$\varepsilon_{V,\text{thermal}} = 3\alpha_T \Delta\theta \tag{8}$$

where $\Delta\theta$ is the temperature change. Assuming a thermal expansion coefficient of $180 \cdot 10^{-6}$ K^{-1} and a temperature increase of 50 K in the PP material, the volumetric strain due to self-heating is determined to be 0.9%, which is negligible compared to the substantial volumetric strain from deformation. Considering XLPE, we assume a thermal expansion coefficient of $200 \cdot 10^{-6}$ K^{-1} and a temperature increase of 30 K. This assumption provides a thermal volumetric strain of 0.6%, which is approximately 30% of the maximum volumetric strain ($\approx 2\%$) at room temperature (Figure 9a).

4.5. Network hardening and locking stretch

An interesting observation for the PP material is that the characteristic network hardening, caused by the alignment of the polymer chains, does not occur for the highest strain rate ($\dot{e} = 1.0$ s^{-1}) at the two lowest temperatures ($T = -15$ °C and $T = -30$ °C). This result is due to the formation of an unstable neck, as shown by the Considère construction in Figure 24, which presents graphs of the functions $\sigma(\varepsilon_L)$ and $\Theta(\varepsilon_L)$, where $\Theta = d\sigma/d\varepsilon_L$ is the hardening modulus. The function $\Theta(\varepsilon_L)$ is found by numerical differentiation of $\sigma(\varepsilon_L)$ and then smoothed. It is evident that the graph of $\Theta(\varepsilon_L)$ crosses the graph of $\sigma(\varepsilon_L)$ twice for the uniaxial tension test performed at room temperature, whereas for the three lower temperatures, there is only one intersection – indicating an unstable neck. An explanation for this result may be found by examining the volumetric strain vs. longitudinal strain curves in Figure 15. At room temperature, a peak value is reached before the volumetric strain decreases. This result indicates, as previously depicted in Figure 16, that voids in the material grow up to a certain point before they are stabilized or start to collapse. At the lower temperatures, however, the voids only continue to grow up to fracture, which in effect inhibits the

16

formation of a stable neck. This is also supported by the observed reduction in the overall ductility of the tensile specimen, as shown by the two photographs in Figure 25.

The influence of rate and temperature on the locking stretch can be analyzed by application of the expression proposed by Arruda et al. [4], viz.

$$\mu(\theta)N(\theta) = \text{constant} \tag{9}$$

where $\mu(\theta)$ is the temperature-dependent shear modulus and $N(\theta)$ is the temperature-dependent number of statistical rigid links per chain. Equation (9) also conserves the number of rigid links (cross-links in the XLPE material and entanglements in the PP material), and hence preserves the mass of the system. The number of statistical rigid links per chain, N, is related to the locking stretch as $\lambda_{\text{lock}} = \sqrt{N}$. Young's modulus, and consequently the shear modulus, increases with decreasing temperature for both materials, as shown in Figures 20 and 21. Equation (9) then implies that the locking stretch increases with temperature. Investigating the locking stretch at increasing strain rates while keeping the temperature fixed, we see from Figures 8 and 14 that the implication of Equation (9) holds, i.e., the locking stretch increases at elevated strain rates due to self-heating in the material (Figures 11 and 17). Exceptions are PP at the highest strain rate, which fails to form a stable neck below a temperature of $T = 0\,°\text{C}$, and XLPE at a temperature of -30 °C, where network hardening does not occur at the two highest strain rates.

Considering isothermal conditions ($\dot{e} = 0.01\ \text{s}^{-1}$), the implications of Equation (9) hold for PP, where we find that the locking stretch decreases and Young's modulus increases when the temperature decreases. However, for XLPE, we find that Young's modulus increases for decreasing temperatures, but a less significant effect is observed in terms of the locking stretch.

5. Conclusions

The following conclusions are drawn:

- The influence of strain rate and temperature on the mechanical behaviour of PP and XLPE in tension and compression was studied experimentally. We observed that the yield stress in tension relates to the temperature and strain rate through the Ree-Eyring flow theory and that Young's modulus follows an exponential relation with decreasing temperature within the experimental range. This finding holds for both materials.

17

- In terms of self-heating, a substantial temperature increase is observed in both materials at the elevated strain rates. At the highest strain rate ($\dot{e} = 1.0 \text{ s}^{-1}$), a continuous temperature increase indicates that we have close to adiabatic conditions, whereas for the lowest strain rate ($\dot{e} = 0.01 \text{ s}^{-1}$) isothermal conditions are met.

- The polypropylene material exhibits substantial volumetric strains, ranging from 0.6 to 0.9. This is believed to be caused by cavitation in the rubbery phase of the material. A change in the evolution of the volumetric strain is also observed at the highest strain rates when decreasing the temperature. At room temperature, the volumetric strain increases until it reaches a maximum value, after which it starts to decrease. SEM micrographs suggest that this behaviour is caused by the stabilization of the growing voids when the material hardens due to large strains, causing the voids to collapse. However, this does not occur at the lower temperatures, which could be caused by the loss of ductility, facilitating coalescence rather than void collapse. In the polyethylene material, the volumetric strain remains small at room temperature but increases when the temperature is lowered.

- Pressure sensitivity, defined as the ratio between the compressive and tensile yield stress ($\alpha_p = \sigma_C/\sigma_T$), is found to be substantial for the PP material, ranging from a minimum value of 1.22 at room temperature and the lowest strain rate to 1.71 at a temperature of $-15\ ^\circ\text{C}$ and the highest strain rate. This difference in yield stress in the two deformation modes is due to the formation of voids in tension, a phenomenon that does not occur in compression. In the XLPE material, however, where the volumetric strain remains small, the pressure sensitivity parameter is close to unity for all test configurations.

6. Acknowledgements

References

[1] F. Grytten, H. Daiyan, M. Polanco-Loria, S. Dumoulin, Use of digital image correlation to measure large-strain tensile properties of ductile thermoplastics, Polymer Testing 28 (6) (2009) 653–660. `doi:10.1016/j.polymertesting.2009.05.009`.

[2] V. Delhaye, A. H. Clausen, F. Moussy, R. Othman, O. S. Hopperstad, Influence of stress state and strain rate on the behaviour of a rubber-particle reinforced polypropylene, International Journal of Impact Engineering 38 (4) (2011) 208–218. `doi:10.1016/j.ijimpeng.2010.11.004`.

[3] M. Jerabek, Z. Major, R. W. Lang, Strain determination of polymeric materials using digital image correlation, Polymer Testing 29 (3) (2010) 407–416. `doi:10.1016/j.polymertesting.2010.01.005`.

[4] E. M. Arruda, M. C. Boyce, R. Jayachandran, Effects of strain rate, temperature and thermomechanical coupling on the finite strain deformation of glassy polymers, Mechanics of Materials 19 (2-3) (1995) 193–212. `doi:10.1016/0167-6636(94)00034-E`.

[5] J. Zaroulis, M. Boyce, Temperature, strain rate, and strain state dependence of the evolution in mechanical behaviour and structure of poly(ethylene terephthalate) with finite strain deformation, Polymer 38 (6) (1997) 1303–1315. `doi:10.1016/S0032-3861(96)00632-5`.

[6] L. C. A. Van Breemen, T. A. P. Engels, E. T. J. Klompen, D. J. A. Senden, L. E. Govaert, Rate- and temperature-dependent strain softening in solid polymers, Journal of Polymer Science, Part B: Polymer Physics 50 (24) (2012) 1757–1771. `doi:10.1002/polb.23199`.

[7] F. Zaïri, M. Naït-Abdelaziz, J. M. Gloaguen, J. M. Lefebvre, Constitutive modelling of the large inelastic deformation behaviour of rubber-toughened poly(methyl methacrylate): effects of strain rate, temperature and rubber-phase volume fraction, Modelling and Simulation in Materials Science and Engineering 18 (5) (2010) 055004. `doi:10.1088/0965-0393/18/5/055004`.

[8] M. Nasraoui, P. Forquin, L. Siad, A. Rusinek, Influence of strain rate, temperature and adiabatic heating on the mechanical behaviour of poly-methyl-methacrylate: Experimental and modelling analyses, Materials and Design 37 (2012) 500–509. `doi:10.1016/j.matdes.2011.11.032`.

[9] V. Srivastava, S. A. Chester, N. M. Ames, L. Anand, A thermo-mechanically-coupled large-deformation theory for amorphous polymers in a temperature range which spans their glass transition, International Journal of Plasticity 26 (8) (2010) 1138–1182. `doi:10.1016/j.ijplas.2010.01.004`.

[10] J. Richeton, S. Ahzi, K. Vecchio, F. Jiang, R. Adharapurapu, Influence of temperature and strain rate on the mechanical behavior of three amorphous polymers: Characterization and modeling of the compressive yield stress, International Journal of Solids and Structures 43 (7-8) (2006) 2318–2335. `doi:10.1016/j.ijsolstr.2005.06.040`.

[11] K. Cao, Y. Wang, Y. Wang, Effects of strain rate and temperature on the tension behavior of polycarbonate, Materials and Design 38 (2012) 53–58. `doi:10.1016/j.matdes.2012.02.007`.

[12] E. N. Brown, P. J. Rae, E. B. Orler, The influence of temperature and strain rate on the constitutive and damage responses of polychlorotrifluoroethylene (PCTFE, Kel-F 81), Polymer 47 (21) (2006) 7506–7518. `doi:10.1016/j.polymer.2006.08.032`.

[13] D. A. Şerban, G. Weber, L. Marşavina, V. V. Silberschmidt, W. Hufenbach, Tensile properties of semi-crystalline ther-

19

moplastic polymers: Effects of temperature and strain rates, Polymer Testing 32 (2) (2013) 413–425. `doi:10.1016/j.` `polymertesting.2012.12.002.`

[14] C. Bauwens-Crowet, The compression yield behaviour of polymethyl methacrylate over a wide range of temperatures and strain-rates, Journal of Materials Science 8 (7) (1973) 968–979. `doi:10.1007/BF00756628.`

[15] M. Ponçot, F. Addiego, A. Dahoun, True intrinsic mechanical behaviour of semi-crystalline and amorphous polymers: Influences of volume deformation and cavities shape, International Journal of Plasticity 40 (2013) 126–139. `doi:10.1016/j.` `ijplas.2012.07.007.`

[16] J. L. Jordan, D. T. Casem, J. M. Bradley, A. K. Dwivedi, E. N. Brown, C. W. Jordan, Mechanical Properties of Low Density Polyethylene, Journal of Dynamic Behavior of Materials 2 (2016) 411–420. `doi:10.1007/s40870-016-0076-0.`

[17] E. N. Brown, R. B. Willms, G. T. Gray, P. J. Rae, C. M. Cady, K. S. Vecchio, J. Flowers, M. Y. Martinez, Influence of molecular conformation on the constitutive response of polyethylene: A comparison of HDPE, UHMWPE, and PEX, Experimental Mechanics 47 (2007) 381–393. `doi:10.1007/s11340-007-9045-9.`

[18] F. Addiego, A. Dahoun, C. G'Sell, J. M. Hiver, Characterization of volume strain at large deformation under uniaxial tension in high-density polyethylene, Polymer 47 (2006) 4387–4399. `doi:10.1016/j.polymer.2006.03.093.`

[19] J. Johnsen, F. Grytten, O. S. Hopperstad, A. H. Clausen, Experimental set-up for determination of the large-strain tensile behaviour of polymers at low temperatures, Polymer Testing 53 (2016) 305–313. `doi:10.1016/j.polymertesting.` `2016.06.011.`

[20] T. Ree, H. Eyring, Theory of non-Newtonian flow. I. Solid plastic system, Journal of Applied Physics 26 (7) (1955) 793–800. `doi:10.1063/1.1722098.`

[21] A. Lazzeri, C. B. Bucknall, Dilatational bands in rubber-toughened polymers, Journal of Materials Science 28 (1993) 6799–6808. `doi:10.1007/BF00356433.`

[22] A. Steenbrink, E. Van der Giessen, On cavitation, post-cavitation and yield in amorphous polymerrubber blends, Journal of the Mechanics and Physics of Solids 47 (1999) 843–876. `doi:10.1016/S0022-5096(98)00075-1.`

[23] Borcoat EA165E, `http://www.borealisgroup.com/en/polyolefins/products/Borcoat/Borcoat-EA165E/`, accessed:2016-1116.

[24] Borlink LS4201S, `http://www.borealisgroup.com/en/polyolefins/products/Borlink/Borlink-LS4201S/`, accessed:2016-1116.

[25] ISO22007-4:2008, Plastics - Determination of thermal conductivity and thermal diffusivity - Part 4: Laser flash method, 2008.

[26] M. Andersen, An experimental and numerical study of thermoplastics at large deformations, Ph.D. thesis, Norwegian University of Science and Technology, NTNU (2016).

[27] E. Fagerholt, T. Børvik, O. S. Hopperstad, Measuring discontinuous displacement fields in cracked specimens using digital image correlation with mesh adaptation and crack-path optimization, Optics and Lasers in Engineering 51 (3) (2013) 299–310. `doi:10.1016/j.optlaseng.2012.09.010.`

[28] J. L. Halary, F. Laupretre, L. Monnerie, Polymer Materials: Macroscopic Properties and Molecular Interpretations, John Wiley & Sons, Inc., Hoboken, New Jersey, 2011, Ch. 9, p. 167.

[29] D. J. A. Senden, S. Krop, J. A. W. van Dommelen, L. E. Govaert, Rate- and temperature-dependent strain hardening of polycarbonate, Journal of Polymer Science, Part B: Polymer Physics 50 (24) (2012) 1680–1693. `doi:10.1002/polb.`

23165.

[30] W. D. Callister Jr., D. G. Rethwisch, Materials Science and Engineering, 8th Edition, John Wiley & Sons, Inc., 2011, Ch. Appendix B, p. A19.
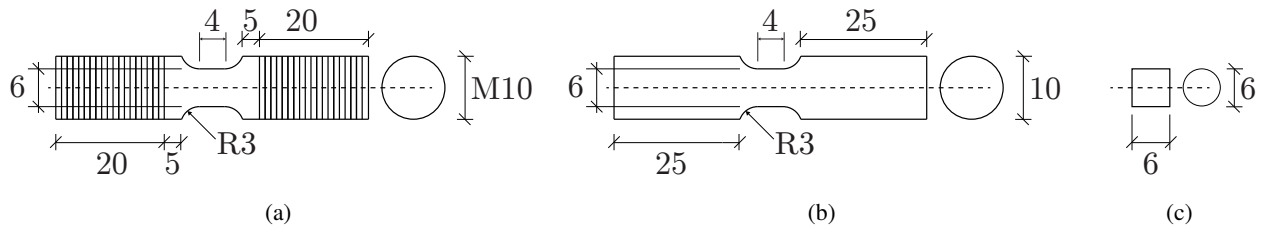
Figure 1: Schematics of (a) tensile test specimen for the PP material, (b) tensile test specimen for the XLPE material, and (c) compression test specimen for both materials. All measures are in mm.
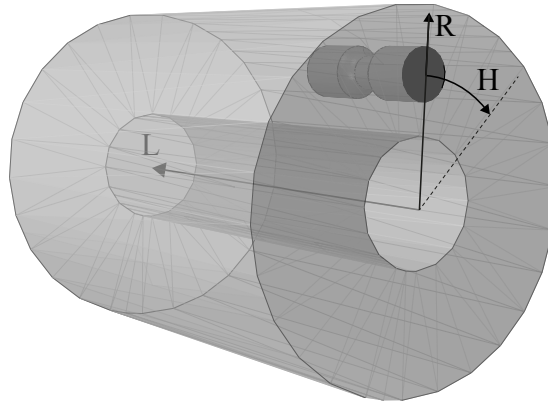
Figure 2: Illustration of the different directions used for the tension and compression specimens, where L, R, and H are the longitudinal, radial and hoop directions, respectively.

Figure 3: Illustration of the experimental set-up. The back-lighted sheets of paper were used to obtain good contrast between the specimen and the surroundings. All measures are in mm.

Figure 4: Absolute logarithmic transverse strains in the radial ($|\varepsilon_R|$) and the hoop ($|\varepsilon_H|$) directions as functions of logarithmic longitudinal strain (ε_L) for both materials. All curves are from tension experiments at room temperature and the lowest strain rate.

Figure 5: (a) Typical speckle pattern on a tensile specimen and (b) typical surface points on a compression specimen. The red squares indicate the two points that were used to calculate the longitudinal strain in the compression tests. All measures are in mm.

(a)

(b)
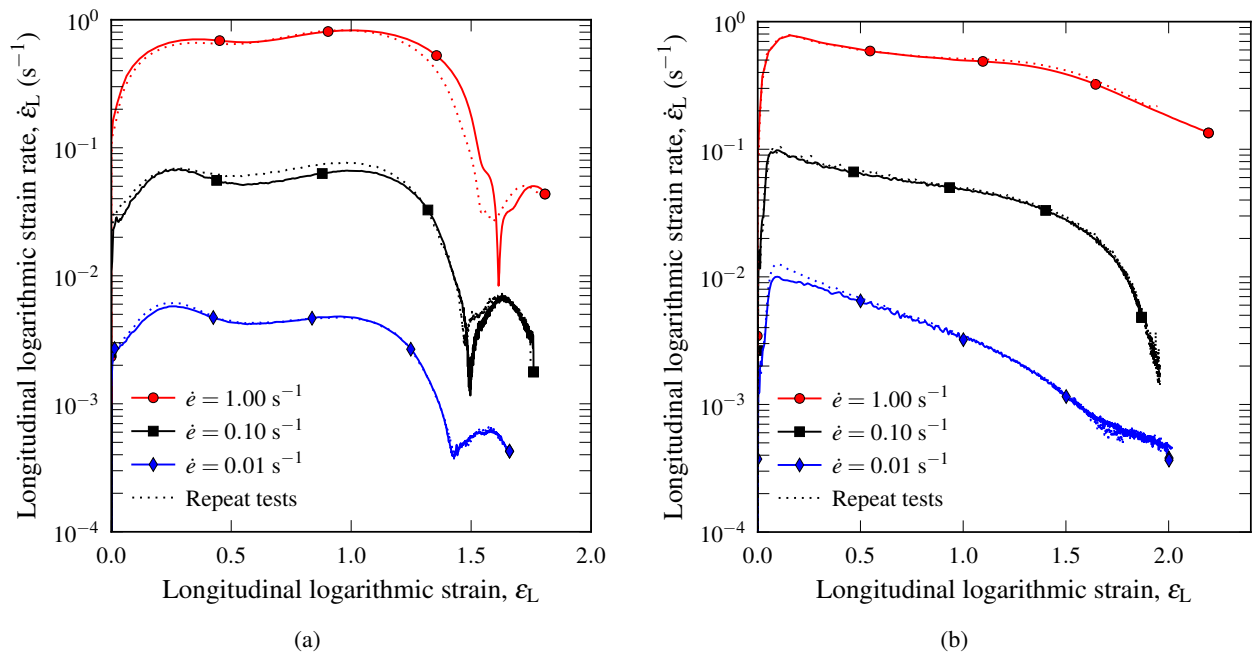
Figure 6: Longitudinal logarithmic strain rate ($\dot{\varepsilon}_L$) at room temperature for (a) the XLPE material and (b) the PP material as a function of longitudinal logarithmic strain.
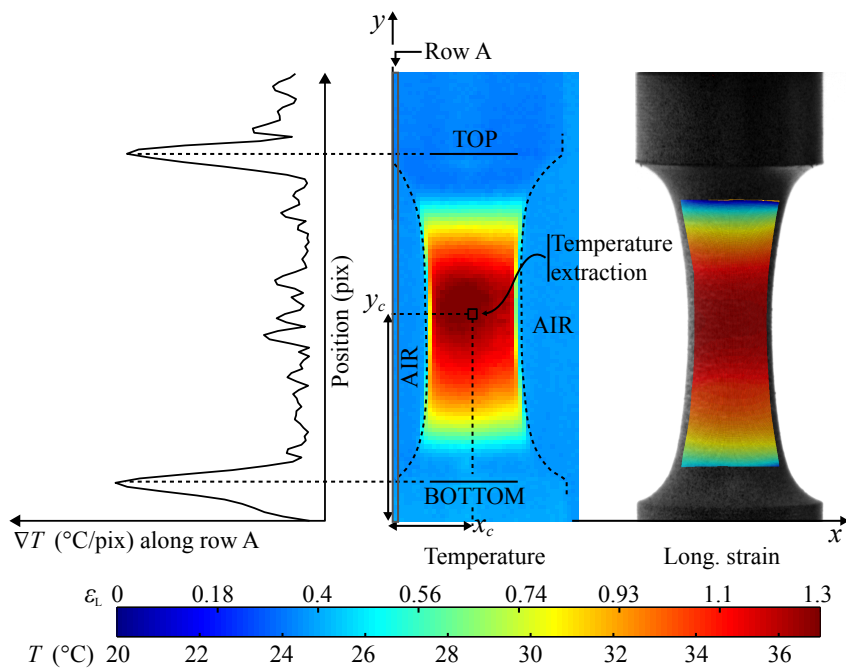
Figure 7: Temperature field from the IR camera alongside the longitudinal strain field from a tension test on PP at room temperature ($T = 25\,^\circ$C) and a strain rate $\dot{e}$ of $1.0\ \mathrm{s}^{-1}$. The temperature gradient, ∇T, is calculated along row A to find the top and bottom of the specimen. The temperature was extracted at the position marked with a square. Dashed lines are guides to the eye showing the outline of the tensile specimen.
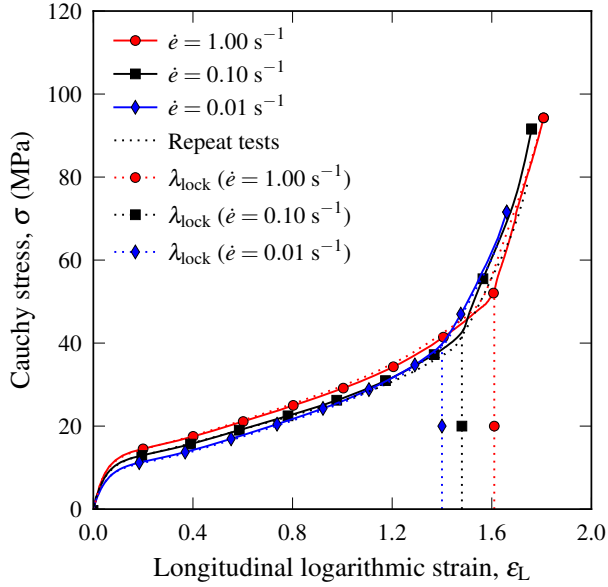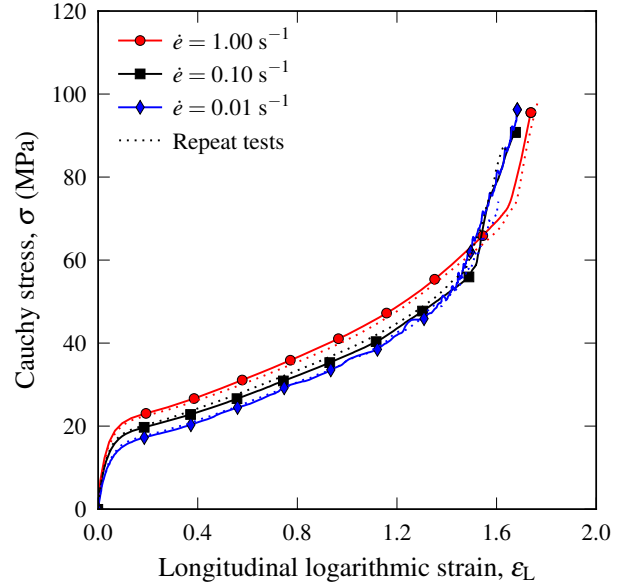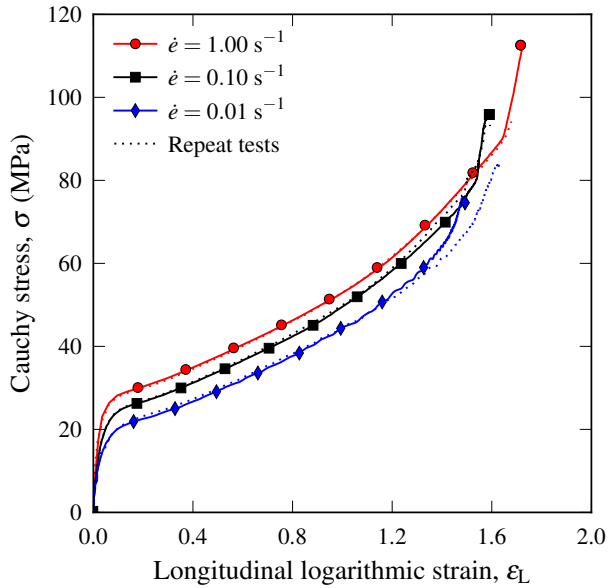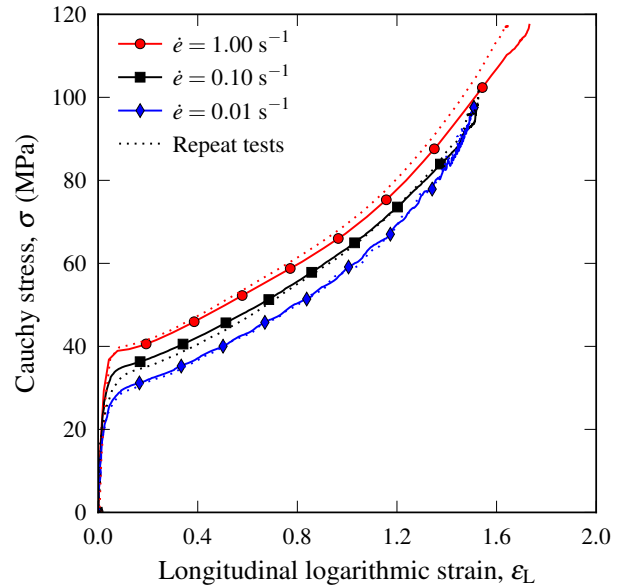
Figure 8: Cross-linked low-density polyethylene (XLPE): Cauchy stress vs. longitudinal logarithmic strain from uniaxial tension tests at three different nominal strain rates, $\dot{e} = 0.01 \text{ s}^{-1}$, $\dot{e} = 0.1 \text{ s}^{-1}$, and $\dot{e} = 1.0 \text{ s}^{-1}$, at four different temperatures, (a) $T = 25\,^{\circ}\text{C}$, (b) $T = 0\,^{\circ}\text{C}$, (c) $T = 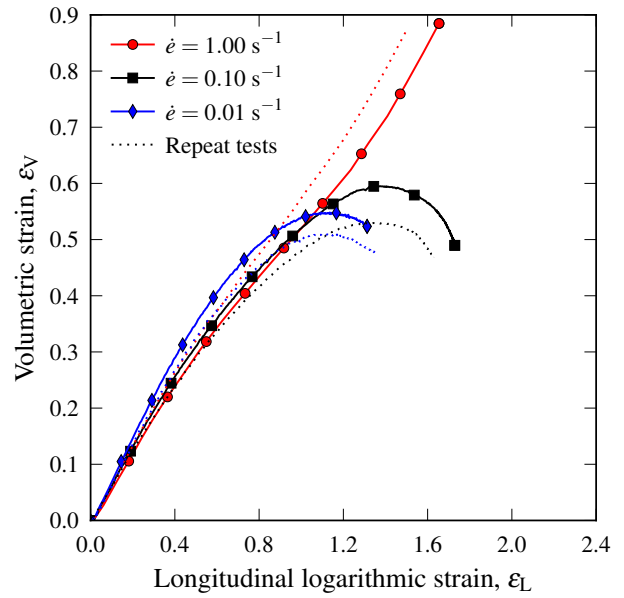-15\,^{\circ}\text{C}$, and (d) $T = -30\,^{\circ}\text{C}$. Note that the repeat tests at the two highest strain rates in (a) were performed with only one digital camera.
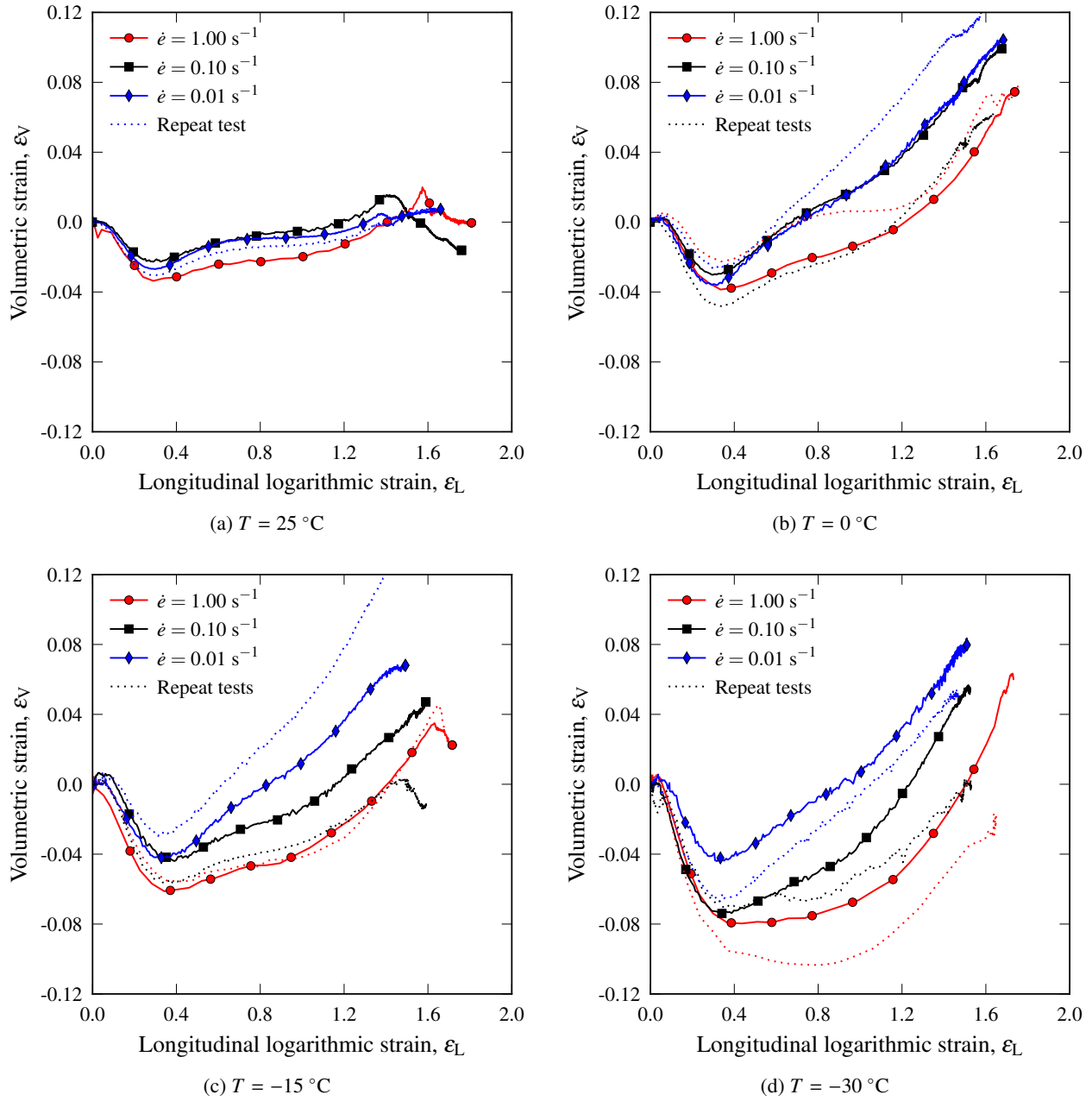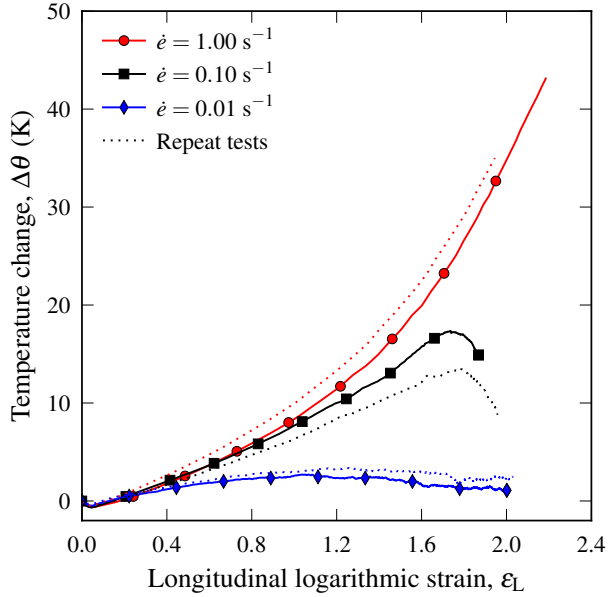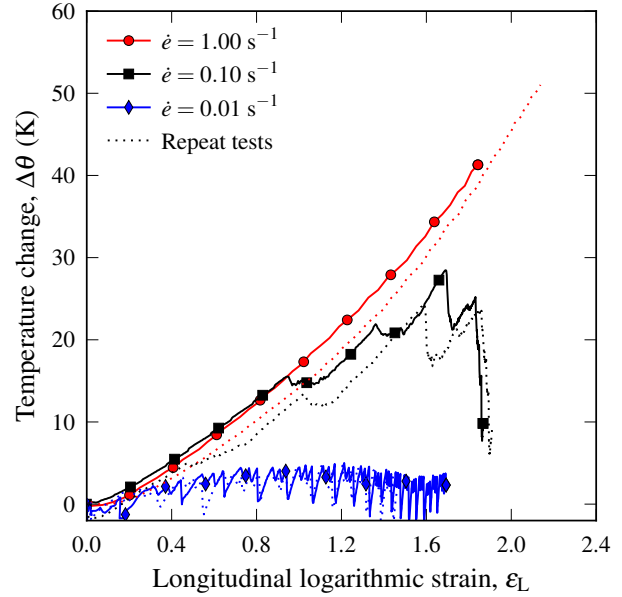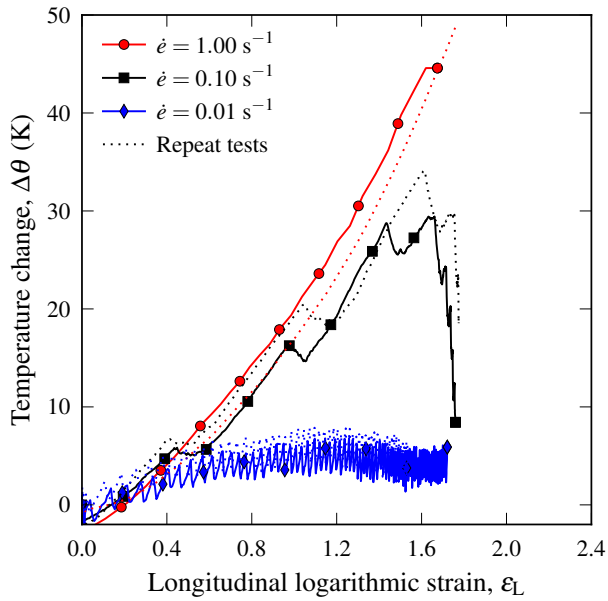
Figure 9: Cross-linked low-density polyethylene (XLPE): Volumetric strain vs. longitudinal logarithmic strain from uniaxial tension tests at three different nominal strain rates, $\dot{e} = 0.01$ s^{-1}, $\dot{e} = 0.1$ s^{-1}, and $\dot{e} = 1.0$ s^{-1}, at four different temperatures, (a) $T = 25$ °C, (b) $T = 0$ °C, (c) $T = -15$ °C, and (d) $T = -30$ °C.

27
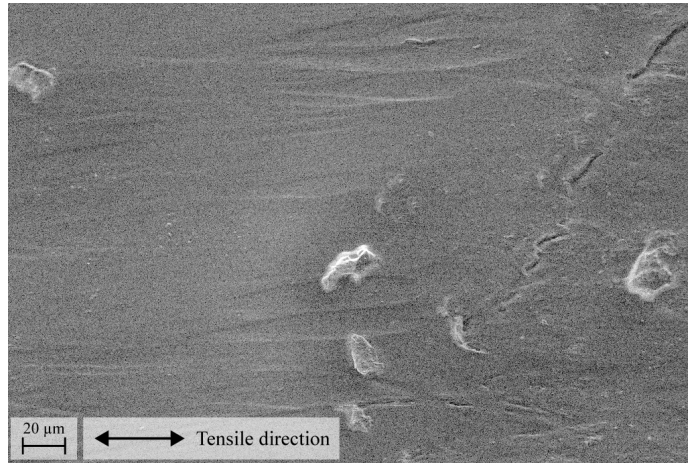
Figure 10: Cross-linked low-density polyethylene (XLPE): Scanning electron microscopy (SEM) micrograph of a tensile specimen loaded to a longitudinal strain of 1.1 and then unloaded.
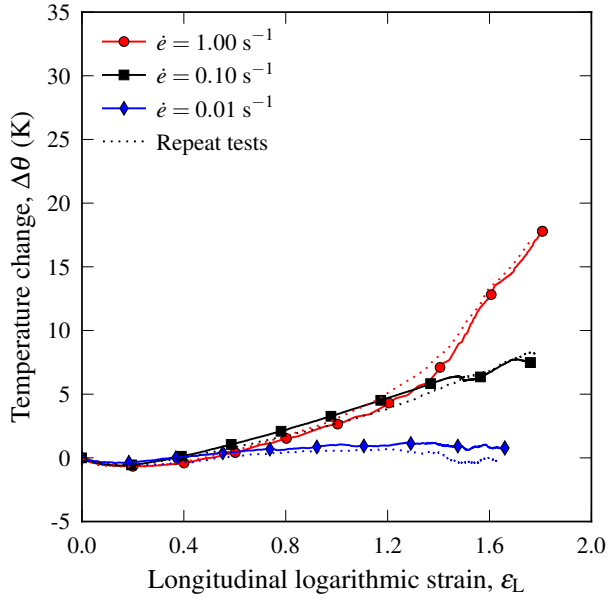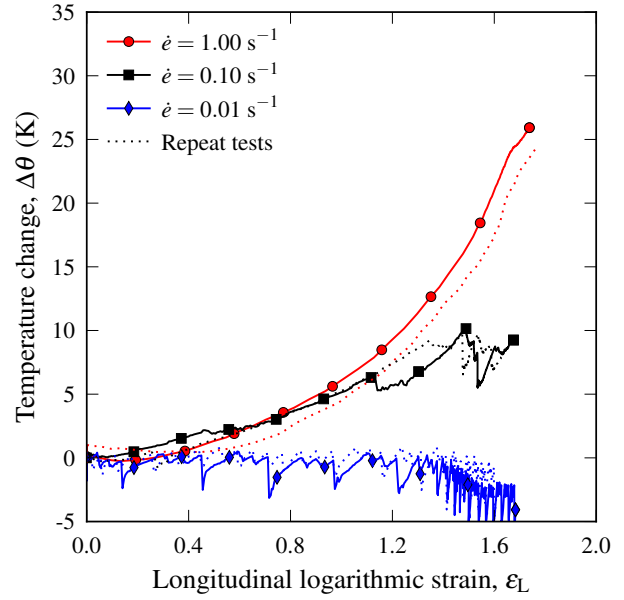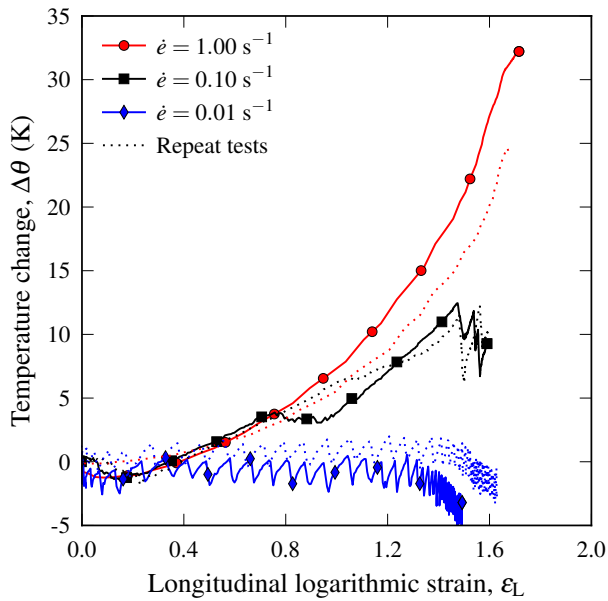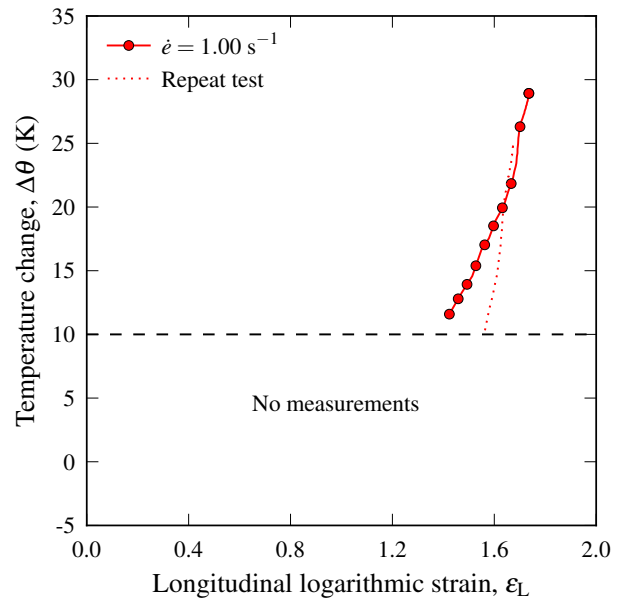
Figure 11: Cross-linked low-density polyethylene (XLPE): Self-heating vs. longitudinal logarithmic strain from uniaxial tension tests at three different nominal strain rates, $\dot{e} = 0.01 \text{ s}^{-1}$, $\dot{e} = 0.1 \text{ s}^{-1}$, and $\dot{e} = 1.0 \text{ s}^{-1}$ at four different temperatures; (a) $T = 25 \text{ °C}$, (b) $T = 0 \text{ °C}$, (c) $T = -15 \text{ °C}$, and (d) $T = -30 \text{ °C}$.
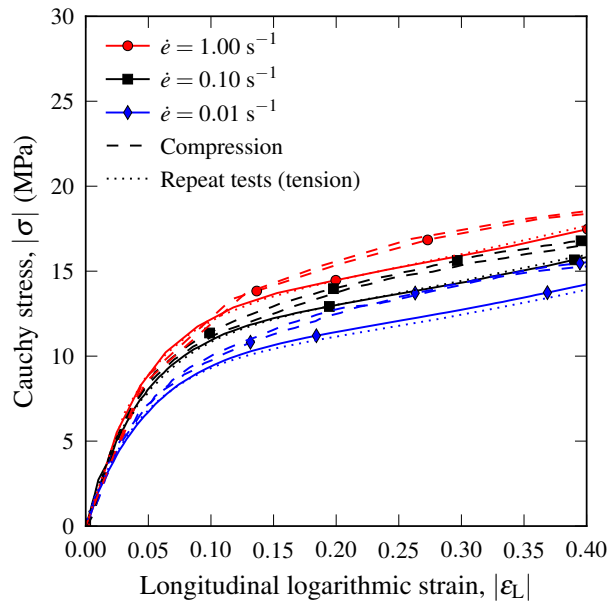
Figure 12: Cross-linked low-density polyethylene (XLPE): Comparison of Cauchy stress vs. longitudinal logarithmic strain curves in compression and tension at T = 25 °C. Note that two repeat tests are given for the compression stress-strain curves.
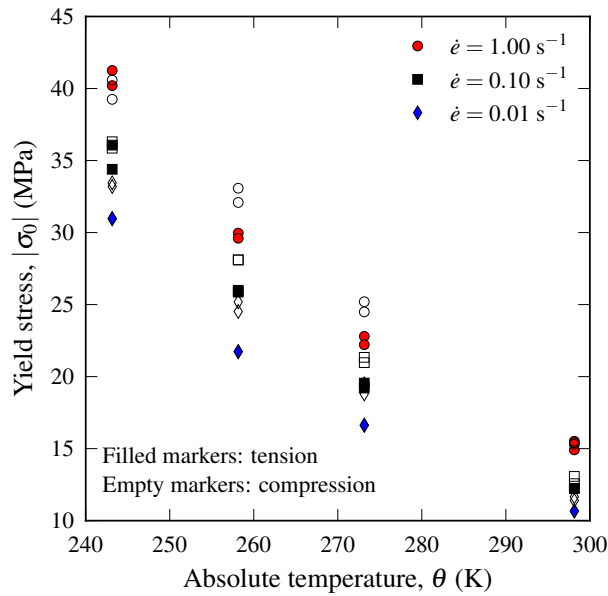
Figure 13: Cross-linked low-density polyethylene (XLPE): Comparison of the tensile and compressive yield stress as a function of temperature and strain rate.
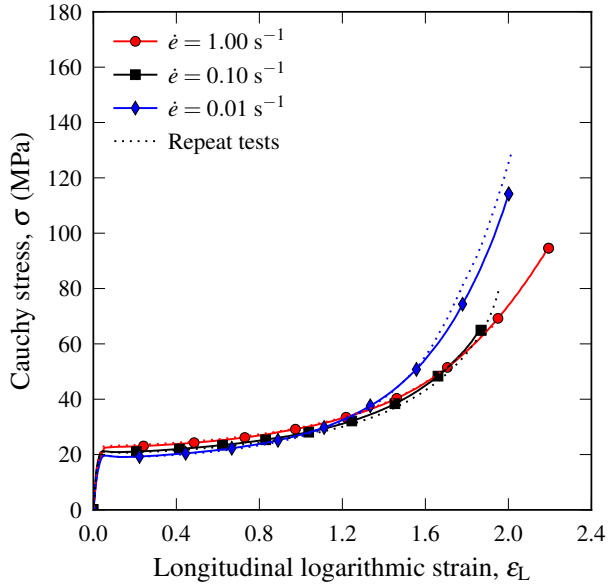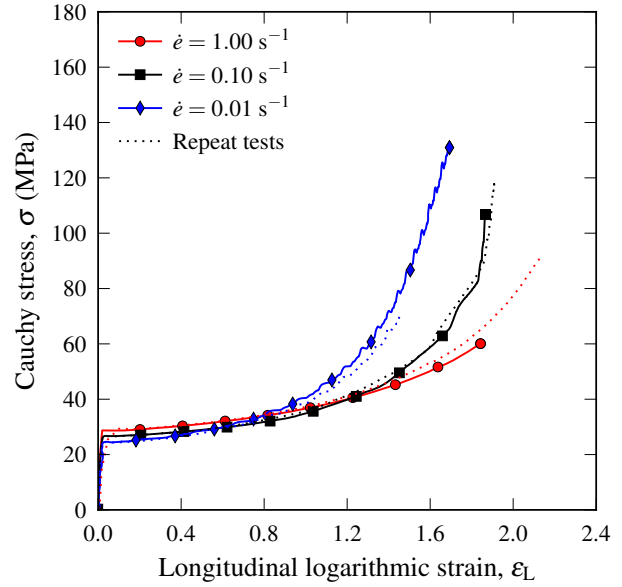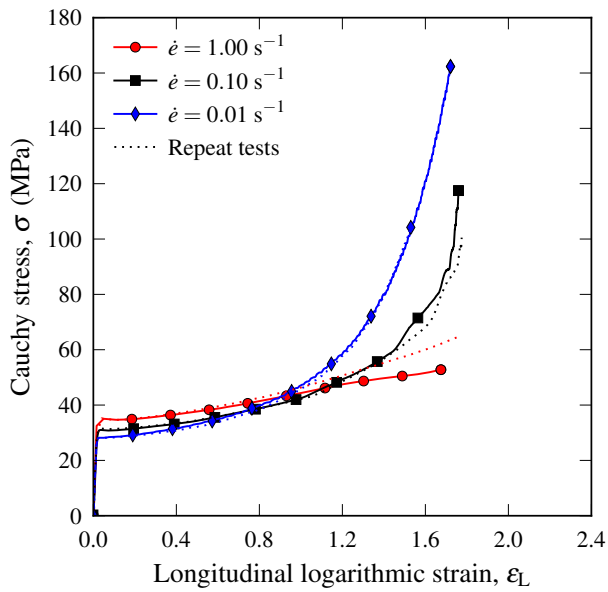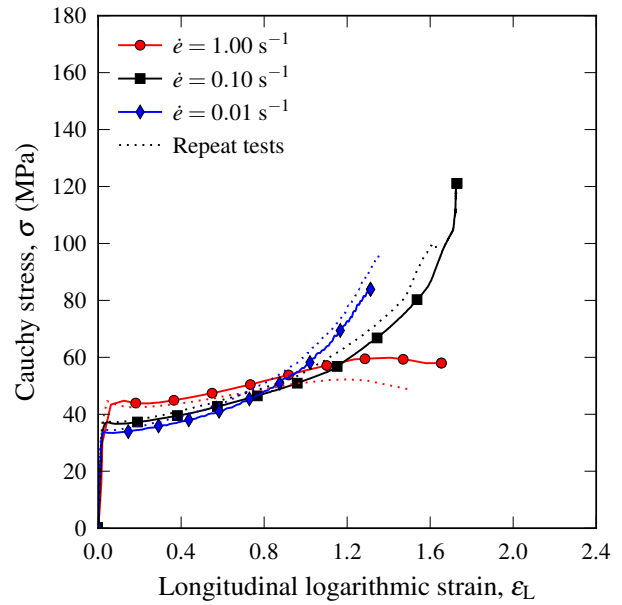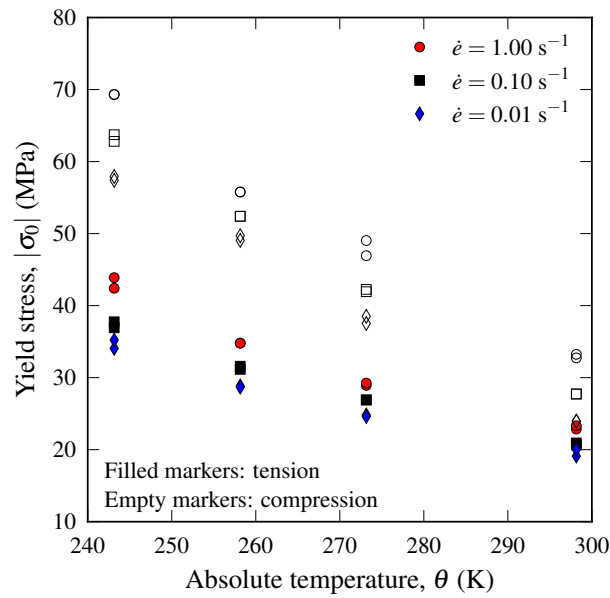
Figure 14: Rubber-modified polypropylene (PP): Cauchy stress vs. longitudinal logarithmic strain from uniaxial tension tests at three different nominal strain rates, $\dot{e} = 0.01\ \mathrm{s}^{-1}$, $\dot{e} = 0.1\ \mathrm{s}^{-1}$, and $\dot{e} = 1.0\ \mathrm{s}^{-1}$, at four different temperatures, (a) $T = 25\ °\mathrm{C}$, (b) $T = 0\ °\mathrm{C}$, (c) $T = -15\ °\mathrm{C}$, and (d) $T = -30\ °\mathrm{C}$.
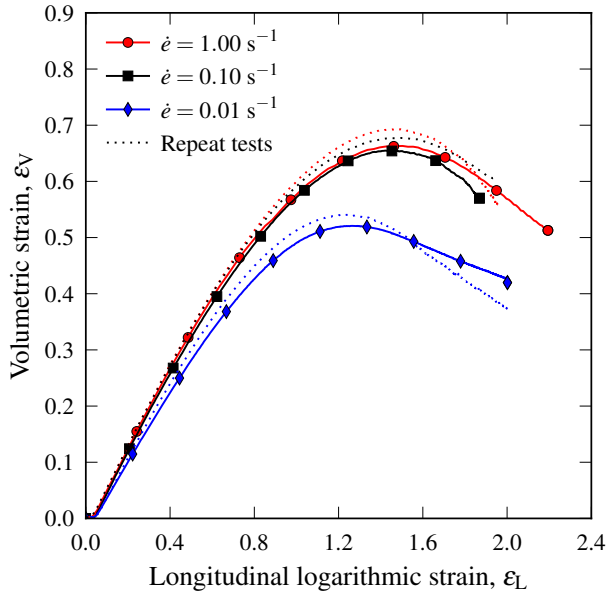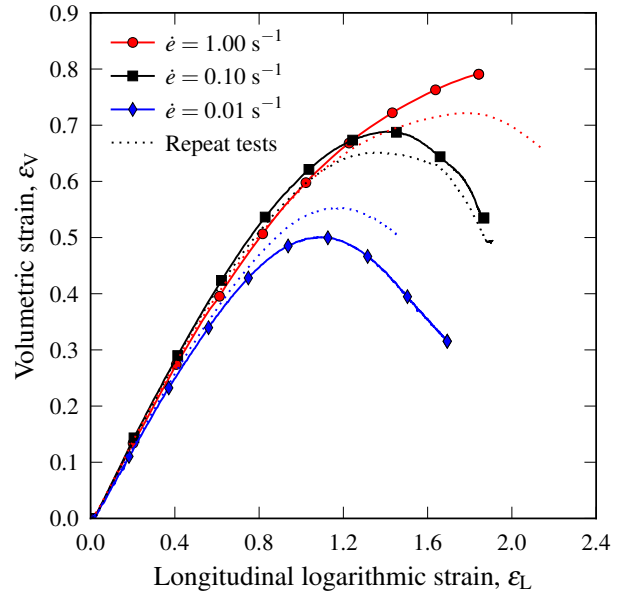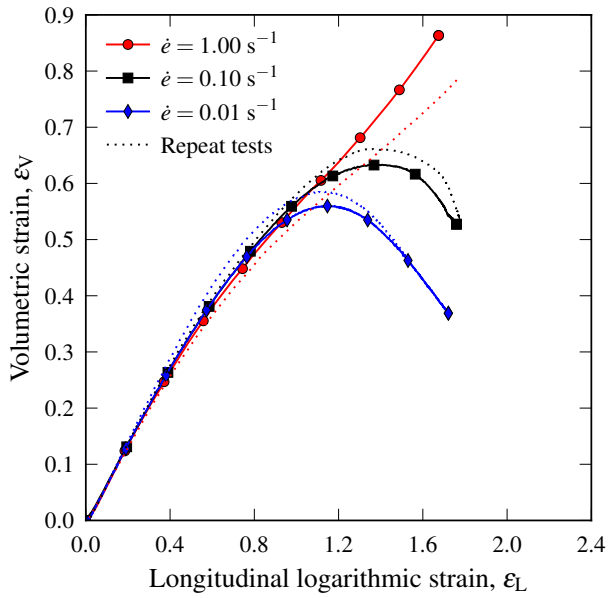
Figure 15: Rubber-modified polypropylene (PP): Volumetric strain vs. longitudinal logarithmic strain from uniaxial tension tests at three different nominal strain rates, $\dot{e} = 0.01$ s^{-1}, $\dot{e} = 0.1$ s^{-1}, and $\dot{e} = 1.0$ s^{-1}, at four different temperatures, (a) $T = 25$ °C, (b) $T = 0$ °C, (c) $T = -15$ °C, and (d) $T = -30$ °C.

32
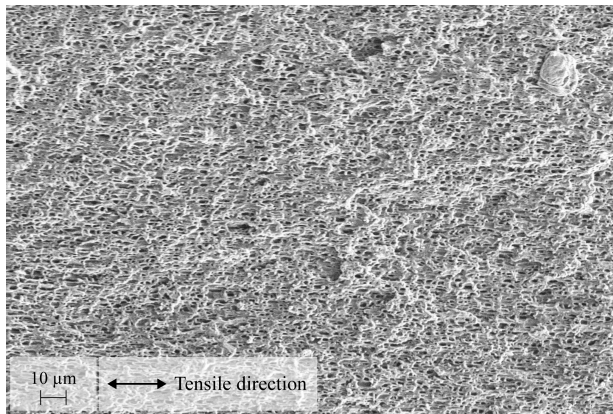
(a)
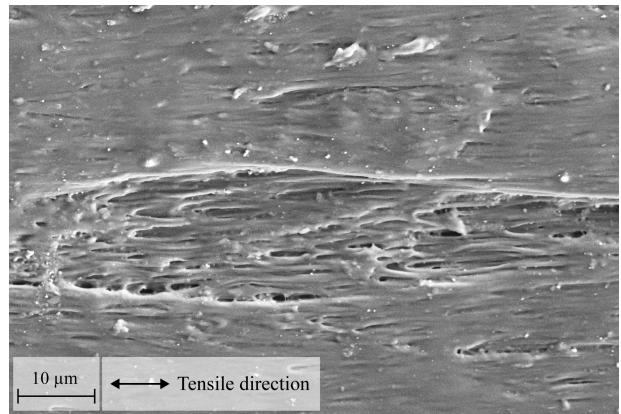
(b)

Figure 16: Rubber-modified polypropylene (PP): Scanning electron microscopy (SEM) micrographs of tensile specimens unloaded (a) before and (b) after peak volumetric strain.
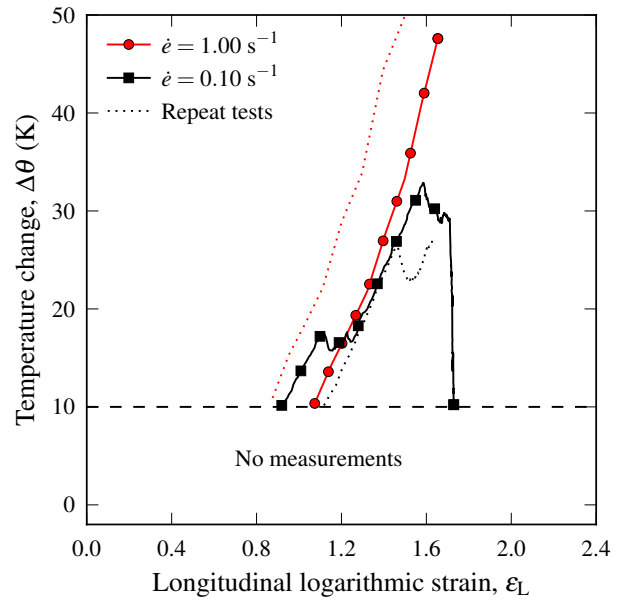
Figure 17: Rubber-modified polypropylene (PP): Self-heating vs. longitudinal logarithmic strain from uniaxial tension tests at three different nominal strain rates, $\dot{e} = 0.01\ \mathrm{s}^{-1}$, $\dot{e} = 0.1\ \mathrm{s}^{-1}$, and $\dot{e} = 1.0\ \mathrm{s}^{-1}$, at four different temperatures, (a) $T = 25\ °\mathrm{C}$, (b) $T = 0\ °\mathrm{C}$, (c) $T = -15\ °\mathrm{C}$, and (d) $T = -30\ °\mathrm{C}$.
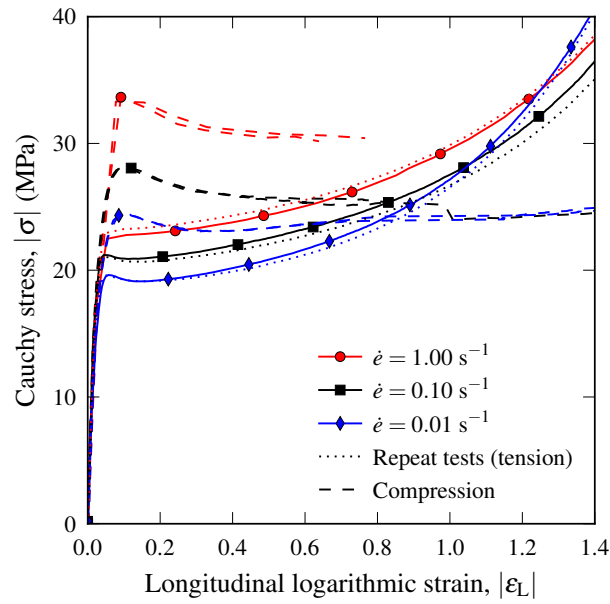
Figure 18: Rubber-modified polypropylene (PP): Comparison of Cauchy stress vs. longitudinal logarithmic strain curves in compression and tension at $T = 25\ °C$. Note that two repeat tests are given for the compression stress-strain curves.

Figure 19: Rubber-modified polypropylene (PP): Comparison of the tensile and compressive yield stress as a function of temperature and strain rate.
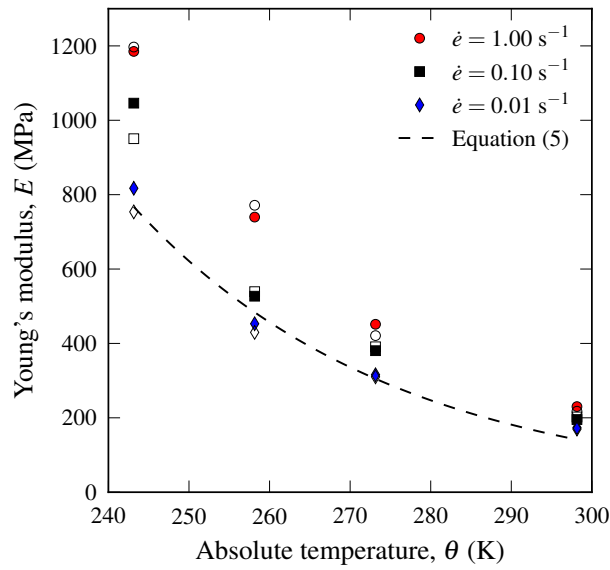
Figure 20: Cross-linked low-density polyethylene (XLPE): Influence of strain rate and temperature on Young's modulus. Equation (5) is fitted only to the Young's moduli at the lowest strain rate. The empty markers are from the repeat tests in Figure 8.
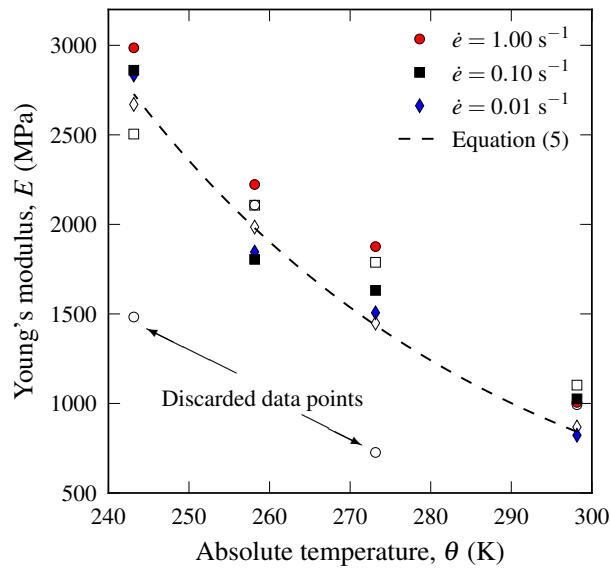
Figure 21: Rubber-modified polypropylene (PP): Influence of strain rate and temperature on Young's modulus. Equation (5) is fitted only to the Young's moduli at the lowest strain rate. The empty markers are from the repeat tests in Figure 14.
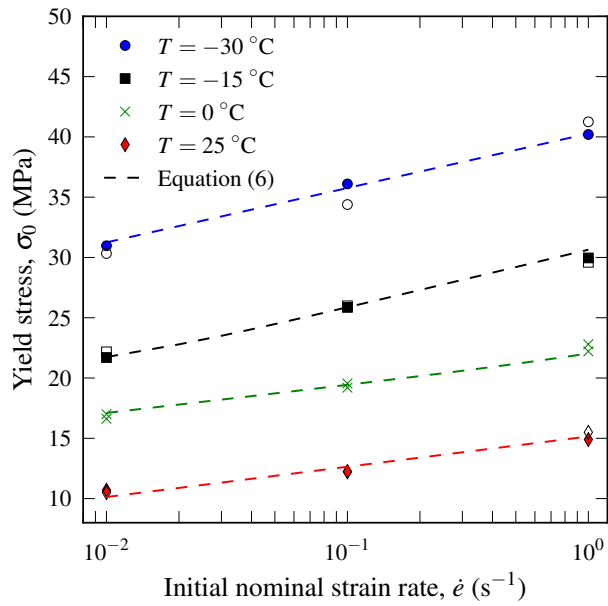
Figure 22: Cross-linked low-density polyethylene (XLPE): Influence of temperature and strain rate on the yield stress. The empty markers are from the repeat tests in Figure 8.
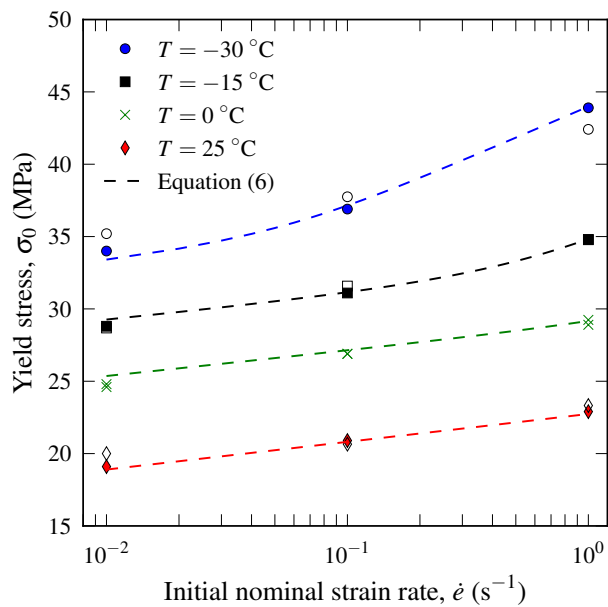
Figure 23: Rubber-modified polypropylene (PP): Influence of temperature and strain rate on the yield stress. The empty markers are from the repeat tests in Figure 14.
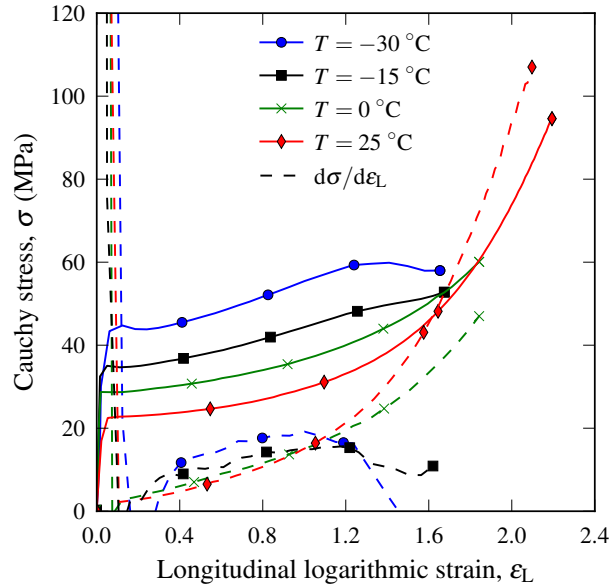
Figure 24: Rubber-modified polypropylene (PP): Considère construction for the uniaxial tension tests at all temperatures for the strain rate $\dot{e} = 1.0\ \mathrm{s}^{-1}$.
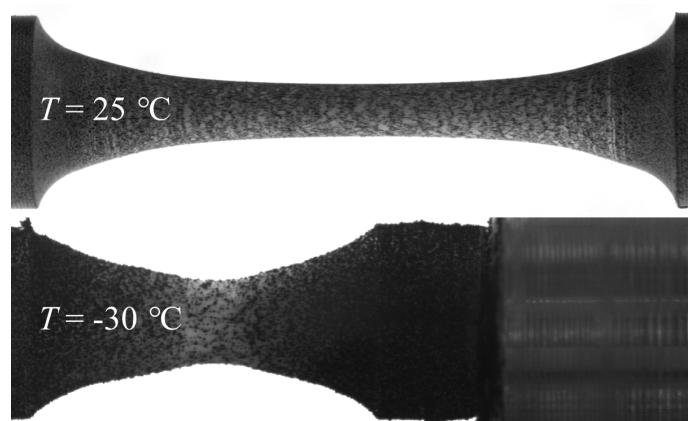
Figure 25: Rubber-modified polypropylene (PP): Comparison of deformed specimens just before fracture in uniaxial tension at $T = 25\ °\mathrm{C}$ (room temperature) and $T = -30\ °\mathrm{C}$ at a strain rate of $\dot{e} = 1.0\ \mathrm{s}^{-1}$.

Table 1: Material properties for the PP and XLPE materials. All parameters are given for room temperature.

Material	Density, ρ (kg/m^3)	Specific heat capacity, C_p (J/(kg·K))	Thermal conductivity, k (W/(m·K))	Heat convection to air, h_c (W/(m^2·K))
XLPE	922	3546	0.56	21
PP	900	2756	0.31	18

Table 2: Pressure sensitivity parameter, $\alpha_p = \sigma_C / \sigma_T$, for the XLPE material.

	$\dot{e}$ (s^{-1})		
T (°C)	0.01	0.1	1.0
25	1.08	1.02	0.98
0	1.13	1.09	1.08
−15	1.13	1.08	1.09
−30	1.08	1.02	0.98

Table 3: Pressure sensitivity parameter, $\alpha_p = \sigma_C / \sigma_T$, for the PP material.

	$\dot{e}$ (s^{-1})		
T (°C)	0.01	0.1	1.0
25	1.22	1.33	1.43
0	1.54	1.56	1.65
−15	1.71	1.67	1.60
−30	1.66	1.69	1.61

Table 4: Material parameters of the Ree-Eyring model, Equation (6).

Material	k_B (J/K)	R (J/(mol·K))	V_α (nm^3)	$\dot{p}_{0,\alpha}$ (s^{-1})	ΔH_α (kJ/mol)	V_β (nm^3)	$\dot{p}_{0,\beta}$ (s^{-1})	ΔH_β (kJ/mol)
XLPE	$1.38 \cdot 10^{-23}$	8.314	3.77	$2.48 \cdot 10^{31}$	211.8	3.14	$6.07 \cdot 10^{37}$	194.8
PP	$1.38 \cdot 10^{-23}$	8.314	1.37	$3.09 \cdot 10^{17}$	86.4	4.95	$3.62 \cdot 10^{38}$	286.0